Am J Cancer Res 2015;5(7):2156-2168
www.ajcr.us /ISSN:2156-6976/ajcr0008396

Original Article

Sunitinib malate (SU-11248) reduces tumour burden and lung metastasis in an intratibial human xenograft osteosarcoma mouse model

Ram Mohan Ram Kumar, Matthias JE Arlt, Aleksandar Kuzmanov, Walter Born, Bruno Fuchs

Department of Orthopaedics, Laboratory for Orthopaedic Research, Balgrist University Hospital, University of Zurich, Zurich, Switzerland

Received March 24, 2015; Accepted June 2, 2015; Epub June 15, 2015; Published July 1, 2015

Abstract: Osteosarcoma is a rare type of cancer that commonly occurs as a primary bone tumour in children and adolescents and is associated with a poor clinical outcome. Despite complex treatment protocols, including chemotherapy combined with surgical resection, the prognosis for patients with osteosarcoma and metastases remains poor and more effective therapies are required. In this study, we evaluated the therapeutic efficacy of sunitinib malate, a wide-spectrum tyrosine kinase inhibitor, in a preclinical mouse model of osteosarcoma. Sunitinib significantly inhibited proliferation, provoked apoptosis and induced G2/M cell cycle arrest in the human osteosarcoma cell lines SaOS-2 and 143B *in vitro*. Importantly, sunitinib treatment significantly reduced tumour burden, microvessel density and suppressed pulmonary metastasis in a 143B cell-derived intratibial osteosarcoma model in SCID mice. Sunitinib significantly decreased primary tumor tissue proliferation and reduced tumor vasculature. Our study indicates that sunitinib has potential for effective treatment of metastasizing osteosarcoma and provides the framework for future clinical trials with sunitinib alone or in combination with conventional and other novel therapeutics aiming at increased treatment efficacy and improved patient outcome.

Keywords: Osteosarcoma, sunitinib malate, tyrosine kinase inhibitor, lung metastasis, intratibial, microvessel

Introduction

Osteosarcoma (OS) is a rare type of cancer associated with a variety of genetic abnormalities. It is characterised by local aggressiveness and a high metastatic potential, which frequently occurs in the early onset of tumour development and results in poor survival of OS patients [1]. OS has an incidence of four to five cases per million individuals per year and occurs mainly in adolescents and young adults, with a second peak incidence in patients over 50 years of age [2]. OS patients diagnosed with localised disease and subjected to state-of-the-art treatment, which includes surgical resection of the primary tumour and neo-adjuvant multidrug combination chemotherapy, have a 5-year survival rate of 70% [3]. Patients with metastatic disease at diagnosis or with recurrent disease, on the other hand, exhibit a 5-year survival rate of only 20% [4]. The lung is the predominant site of OS metastasis and lung lesions are the most common cause of death in OS patients [5]. Attempts to improve therapeutic efficacy by altering chemotherapy and radiotherapy combination treatments, and also altering dose escalations,has not improved OS survival outcomes [6, 7]. Because of the disappointing outcomes of clinical trials involving OS, new therapeutics and new approaches to treat this disease are urgently needed.

Sunitinib malate (SU-11248) is a small molecule tyrosine kinase inhibitor (TKI) that can penetrate cell membranes. It is metabolized by cytochrome P450 3A4 (CYP3A4) to pharmacologically active N-desethyl metabolite SU12662 [8]. It has been shown to have inhibitory activity in a wide spectrum of kinases including platelet- derived growth factor receptors (PDGFRα and PDGFRβ), vascular endothelial growth factor receptors (VEGFR1, VEGFR2 and VEGFR3), stem cell factor receptor (KIT), Fms-like tyrosine kinase-3 (FLT3), colony stimulating factor recep-

tor type 1 (CSF- b1R) and the glial cell-line derived neurotropic factor receptor (RET) [9, 10]. Sunitinib has been shown to be effective in the treatment of many cancers and has recently been approved for the treatment of patients with pancreatic neuroendocrine tumours, renal cell carcinoma (RCC) and in advanced solid tumours such as gastrointestinal stromal tumours (GIST) [11-13]. These findings led us to hypothesize that sunitinib may also suppress tumour growth and metastasis in OS.

The principal aim of the present study was to evaluate in an intratibial osteolytic and spontaneously metastasizing OS mouse model the suppressive effects of sunitinib malate on primary tumour growth and lung metastasis. In this study, we also determined the *in vitro* cytotoxic effects of sunitinib in the human SaOS-2 and 143B OS cell lines and used a LacZ and m-Cherry expressing 143B cell line derivative in the intratibial OS mouse model.

Materials and methods

Cell culture and reagents

The human OS cell lines SaOS-2 (HTB-85), U2OS (HTB-96) and 143B were purchased from American Type Culture Collection (Manassas, VA, USA). All cell lines were cultured at 37°C in a humidified atmosphere of 5% CO_2 in Dulbecco's modified Eagle'smedium (DMEM containing 4.5 g/l glucose) and Ham F12 (Invitrogen, Carlsbad, CA, USA) at a 1:1 ratio supplemented with 10% fetal calf serum. Cell line authentication was performed by multiplex polymerase chain reaction (Microsynth, Switzerland) with a PowerPlex®16HS system (Promega, USA) and the data verified by comparison with those reported in the German Collection of Microorganisms and Cell Cultures database (DSMZ, Braunschweig, Germany). All cells were cultured at 37°C in a humidified atmosphere of 5% CO_2. Sunitinib was purchased from Bio Vision Inc. (San Francisco, CA, USA). For *in vitro* experiments, stock solutions of 100 mM sunitinib in dimethyl sulfoxide were diluted in DMEM to the indicated final concentrations. For the *in vivo* studies, sunitinib was dissolved in carboxymethylcellulose (CMC) solution (CMC 0.5%, NaCl 1.8%, tween 80 0.4% and benzyl alcohol 0.9% in distilled water). All solvents were purchased from Sigma-Aldrich, USA.

Cell proliferation assay

The effects of sunitinib on the growth of OS cell lines were assessed with a WST assay as previously described [14]. The cells were seeded in 96-well plates at a density of 3×10^3 cells/well and allowed to adhere and grow overnight. The cells were then treated or untreated with sunitinib as indicated in the Figure legends and subsequently incubated for 2-3 h with 10 µl per well WST-1 reagent (Roche Diagnostics Corp., Indianapolis, IN, USA). Formazan produced from WST-1 by mitochondrial dehydrogenase in metabolising cells was quantified at 415 nm in a scanning multiwell spectrophotometer (Bio-Rad, Hercules, CA, USA).

Cell cycle analysis

Cell cycle analysis was performed at the Flow Cytometry Facility of the Federal Institute of Technology (ETH) Zurich. The cells were seeded in dishes of 10 cm in diameter at a density of 1.0×10^6 cells per dish. After initial treatment with indicated concentrations of sunitinib for 24 and 48 h, SaOS-2 and 143B cells were treated with trypsin. They were then collected by centrifugation and washed with PBS. Subsequently, the cells were fixed by incubation in ice-cold 70% (v/v) ethanol overnight at 4°C. The cells are then washed with PBS and resuspended in 500 µl of ice-cold PI/RNase staining buffer (BD Pharmingen AG, Allschwil, Switzerland). The resuspended cells were then incubated at 37°C for 30 min in the dark. The samples were analysed with a fluorescence activated cell sorter (FACS; Calibur, BD, USA). Only single cells were analysed and the percentages of cells in individual phases of the cell cycle were calculated using FlowJo software (Ashland, MA, USA).

Western blot

After treatment with sunitinib at the indicated concentrations, OS cell lines were harvested for protein extraction by lysis buffer. The procedures used for western blotting were those described previously [15]. Briefly, aliquots of protein extracts (30 to 40 µg/lane) were separated by SDS-PAGE (BioRad Laboratories, Hercules, CA, USA) and wet-transferred to nitrocellulose membranes (BioRad Laboratories). They were then probed with antibodies to the following proteins: endogenous caspase-3 (Cell

Signaling, 1:1000); cleaved caspase-3 (Novus Biologicals, 1:500); PARP (Cell Signaling, 1:1000); GAPDH (Santa Cruz, 1:1000) probed with secondary isotype specific antibodies tagged with horseradish peroxidase (Santa Cruz). The bound immuno-complexes were detected with Immobilon chemiluminescence substrate (Millipore, Billerica, MA, USA) and visualized with a VersaDoc system (BioRad Laboratories).

cDNA synthesis and expression analysis

Total RNA was isolated from OS cell lines using an RNeasy mini kit (Qiagen, Valencia, CA, USA), and 1 µg of total RNA was used as atemplate for cDNA synthesis with a High-Capacity cDNA Reverse transcription kit (Applied Biosystems, Foster City, CA, USA). For real time PCR (qRT-PCR) analysis three independent RNA preparations from each cell lines were reverse transcribed in a final volume of 10 µl. qRT-PCR was performed using the StepOne Plus Real- Time PCR system (Applied Biosystems, USA) in 96-well plates. qRT-PCR was performed using following primers CyclinD1 Forward: 5'-TGTTC-GTGGCCTCTAAGATGAAG-3'; Reverse: 5'-AGG-TTCCACTTGAGCTT-GTTCAC-3'; human cyclinB1 Forward: 5'-AAGAGCTTTAAACTTTGGTCTGGG-3', Reverse: 5'-CTTTGTAAGTCCTTGATTTA-CCATG-3'. The cDNA and appropriate primers were added to Power SYBR Green PCR master mix (Applied Biosystems, USA) and the samples were pre-incubated as follows: 50°C for 2 min and at 95°C for 10 min, 40 cycles at 95°C for 15 s and at 60°C for 1 min. Relative expression levels of individual gene transcripts were calculated by the comparative cycle threshold (ΔΔCT) method and normalised to GAPDH transcripts.

Retroviral transduction of LacZ expressing 143B cells with mCherry fluorescent protein (143B/LZ+mC)

A pcDNA3.1 plasmid containing a mCherry reporter gene was a generous gift of Professor M. Rudin (Institute of Biomedical Engineering, University and ETH Zurich). The mCherry gene was sub-cloned from this plasmid into a retroviral pQCXIH vector that contained a hygromycin resistance gene. Retroviral particles containing pQCXIH-mCherry were produced in HEK 293T cells and used for infection, as described previously [16]. After infection of LacZ-positive 143B cells as described previously [17], selection of mCherry-positive cells was performed for 1 week in tissue culture medium containing 400 µg/ml of hygromycin (Merck, Darmstadt, Germany). The infection efficacy and the presence of mCherry-positive 143B cells were assessed by fluorescence microscopy (Zeiss Observer Z1, Zeiss Microscopy, Jena, Germany).

Animals

Female 6-7 week old immunosuppressed SCID mice were purchased from Charles River Laboratories (Sulzfeld, Germany) and maintained in individually ventilated cages. Housing and experimental protocols were in accordance with the Swiss Animal Protection Law and in compliance with the regulations of the Veterinärmt, Kanton Zurich. All manipulations were carried out under sterile conditions in a laminar flow hood.

Intratibial injection of 143B/LZ+mC OS cells

Exponentially growing 143-B/LZ+mC cells were harvested by trypsinisation and washed thoroughly with PBS. 5×10^5 cells in 10 µl of PBS were orthotopically injected with a Hamilton syringe into the medullar cavity of the left proximal tibia of the mice. Prior to injection, the tibia plateau was opened by punching with a 26-gauge needle. Tumour growth and osteolysis were monitored by means of X-ray analysis once a week with the Faxitron® MX-20 Specimen Radiography System (Faxitron X-Ray LLC, Lincolnshire, IL, USA). The tumour volume (V) in individual mice was calculated from measurements with a caliper rule of the largest (L) and the smallest (S) perpendicular diameters of the tumour cell-injected and the healthy control leg. V was calculated as the difference between the volume (=0.5 × L × (S) 2) of the tumour leg and the volume of the control leg. The organs and legs of the mice were prepared at sacrifice and primary tumors and metastases were stained with 5-bromo-4-chloro-3-indolyl-β-D-galactoside (X-gal). For the quantification of macro and micrometastases in the lung of individual mice, images of the surface of one lung lobe were taken under a Nikon Eclipse E600 microscope with a Kappa PS 20 C digital camera (Kappa Optronics GmbH, Gleichen, Germany). Indigo-blue stained foci on lung surfaces with a diameter >0.1 mm were defined as macrometastases, and foci with a diameter

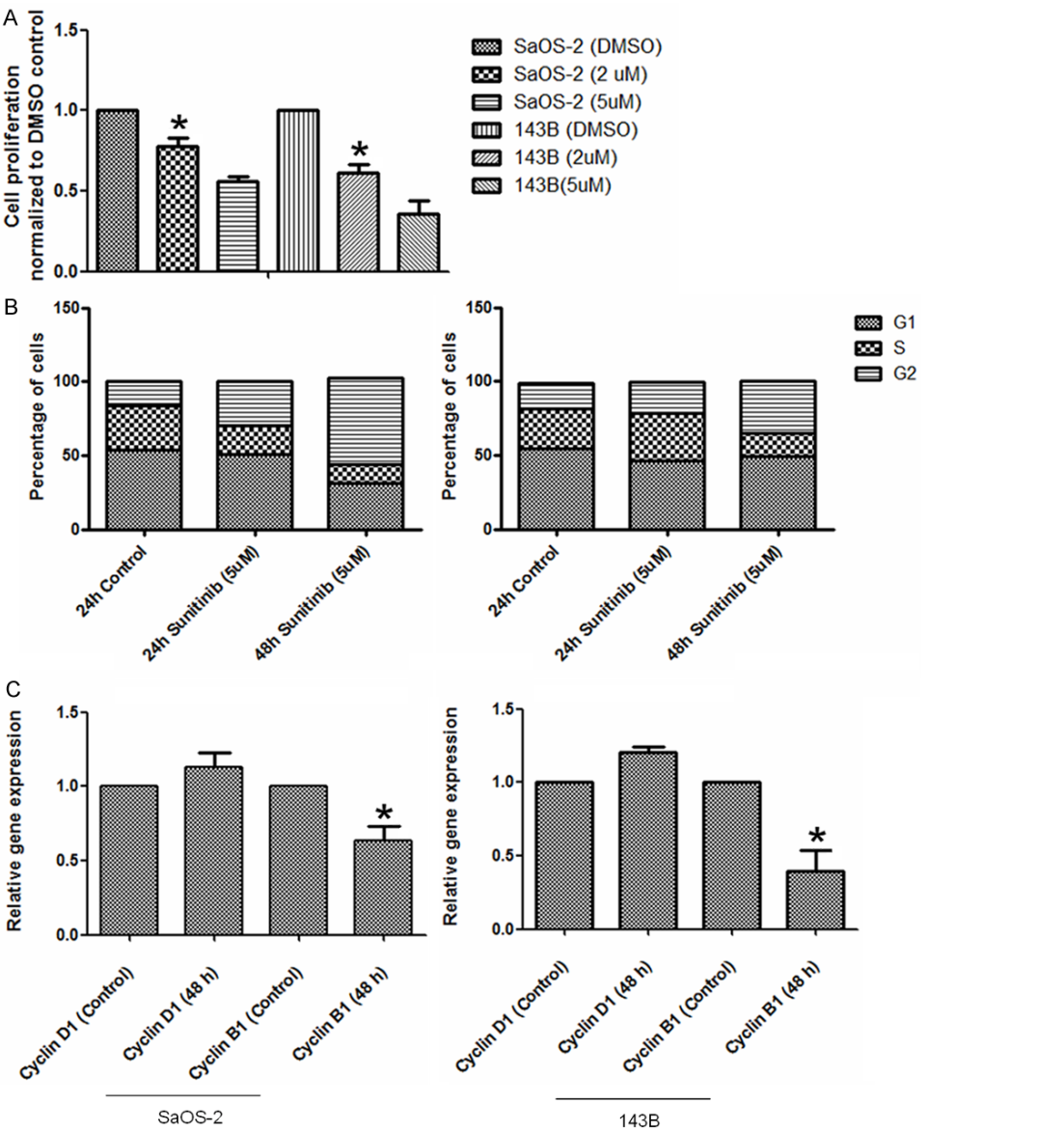
A
Cell proliferation normalized to DMSO control
1.5
1.0
0.5
0.0
*
*
SaOS-2 (DMSO)
SaOS-2 (2 uM)
SaOS-2 (5uM)
143B (DMSO)
143B (2uM)
143B(5uM)
B
Percentage of cells
150
100
50
0
24h Control
24h Sunitinib (5uM)
48h Sunitinib (5uM)
G1
S
G2
C
Relative gene expression
Cyclin D1 (Control)
Cyclin D1 (48 h)
Cyclin B1 (Control)
Cyclin B1 (48 h)
SaOS-2
143B
D
SaOS-2
Control
Sunitinib (5uM)
24h 48h 72h
Caspase 3
Cleaved caspase 3
GAPDH
35 kDa
19 kDa
12 kDa
35 kDa
Full length PARP
Cleaved PARP
GAPDH
116 kDa
89 kDa
35 kDa
45
143B
Control
Sunitinib (5uM)
24h 48h 72h
Caspase 3
Cleaved caspase 3
GAPDH
35 kDa
19 kDa
12 kDa
35 kDa
Full length PARP
Cleaved PARP
GAPDH
116 kDa
89 kDa
35 kDa

Figure 1. Sunitinib malate inhibits growth and induces apoptosis in OS cells *in v*itro. A. SaOS-2 and 143B cells were incubated for 24 h with indicated concentrations of sunitinib or DMSO as a control and proliferation was then assessed by WST-1 assay. Data are the mean ± SEM of three independent experiments normalized to respective DMSO controls (*P<0.05 compared to control). B. Cell cycle analysis of SaOS-2 and 143B cells treated for 24 h and 48 h with indicated concentrations of sunitinib or DMSO as a control. The numbers of cells in indicated growth phases are illustrated in percentage of the total number of cells analysed. C. Analysis of expression of mRNA encoding indicated cell-cycle regulating genes by real time PCR in SaOS-2 and 143B cells treated for 24 h with 5 μM sunitinib or DMSO as a control. The mRNA levels were normalised to those of GAPDH and to controls (n=3) (*P<0.01). D. Western blot analysis of caspase 3 and PARP cleavage in SaOS-2 and 143B cells treated for indicated time periods with sunitinib or DMSO as a control. GAPDH was used as a protein loading control. Representative experiment was carried out three times.

<0.1 mm were defined as micrometastases. The results are presented as the means ± SEM of the number of respective lung metastases counted in atleast ten tumour bearing mice.

Treatment of mice with sunitinib

Sunitinib at dosesof 40 and 80 mg/kg was administered in CMC solution daily with an oral gavage while mice in the control group were treated with CMC solution alone. The treatment of 143B/LZ+mC tumour bearing mice with sunitinib was started when mCherry fluorescent intratibial lesions became detectable by IVIS. The mice (n=30) were then randomly distributed into three groups (control, 40 mg/kg, 80 mg/kg) with 10 mice per group. After treatment for 12 days, all mice were euthanized and their tumours and organs were excised and stored in 4% paraformaldehyde until they were used for immunohistochemical analysis.

In vivo bioluminescent imaging (IVIS) of mCherry fluorescence

Whole body imaging of mCherry fluorescence in mice with 143B/LZ+mC cell-derived intratibial primary tumours was performed weekly with an IVIS imaging system (Caliper Life Sciences, Inc. Hopkinton, MA, USA). Prior to *in-vivo* imaging, the mice were anesthetised with isoflurane. Photon emission was quantified in photons/sec/cm^2 with Living Image 3.1 software (Xenogen Corporation, MA, USA).

Immunohistochemistry (IHC)

Angiogenesis was examined by immunohistochemistry with rabbit polyclonal CD31 antibodies that immunostained vascular endothelial cells (Abcam, UK (dilution 1:250). Briefly, tumour sections were fixed in 4% paraformaldehyde and dehydrated by serial incubation in 70%, 96% and 100% ethanol and xylene and then embedded in paraffin. Tissue sections of 6 μm were mounted onto slides, deparaffinised and rehydrated and then heated in 0.1 M citrate buffer (pH 5.8) for antigen retrieval. Endogenous peroxidase activity was inactivated by incubation of the tissue sections in 3% H_2O_2 for 10 min at RT. The sections were washed with PBS (pH 7) twice, incubated in blocking buffer (10% goat serum and 0.1% Tween in PBS) for 1 h at room temperature and then incubated with CD31 primary antibody (1:150 final dilution) overnight at 4°C. After extensive washing with blocking medium, secondary Alexa Fluor 546-labeled antibodies to rabbit IgG (Life Technologies) at a final dilution of 1:200 were added to the cells and they were incubated for 30 min in the dark. Nuclear DNA was stained with 0.2 μg/ml DAPI (4', 6'-diaminidino-2-phenylindole) (Molecular Probes Inc., Eugene, USA). The coverslips were then washed with PBS and dipped in H_2O and then mounted in Immomount (ThermoScientific; Waltham, MA). Fluorescence was detected with a Nikon Eclipse E600 microscope equipped with appropriate filter blocks (Nikon Corporation, Tokyo, Japan). Ki67 indicating tissue proliferation was immunostained with a rabbit antibody (Abcam, UK) at 1:200 final dilution and secondary anti-rabbit antibodies (1:2000 final dilution) from Santa Cruz. Ki67 immunostained cells were quantified with Image J software.

Microvessel density (MVD) analysis

Rabbit polyclonal CD31 antibody was used as a blood vessel endothelial marker. Vessel density was determined by counting the number of CD31-positive vessels per viable tumour area. Five areas with the highest density of microvessels were viewed at a higher magnification (200 ×) to determine the mean ± SEM of MVD.

Statistical analysis

Data were plotted and analysed using Student's t test. The Prism 4 program (GraphPad soft-

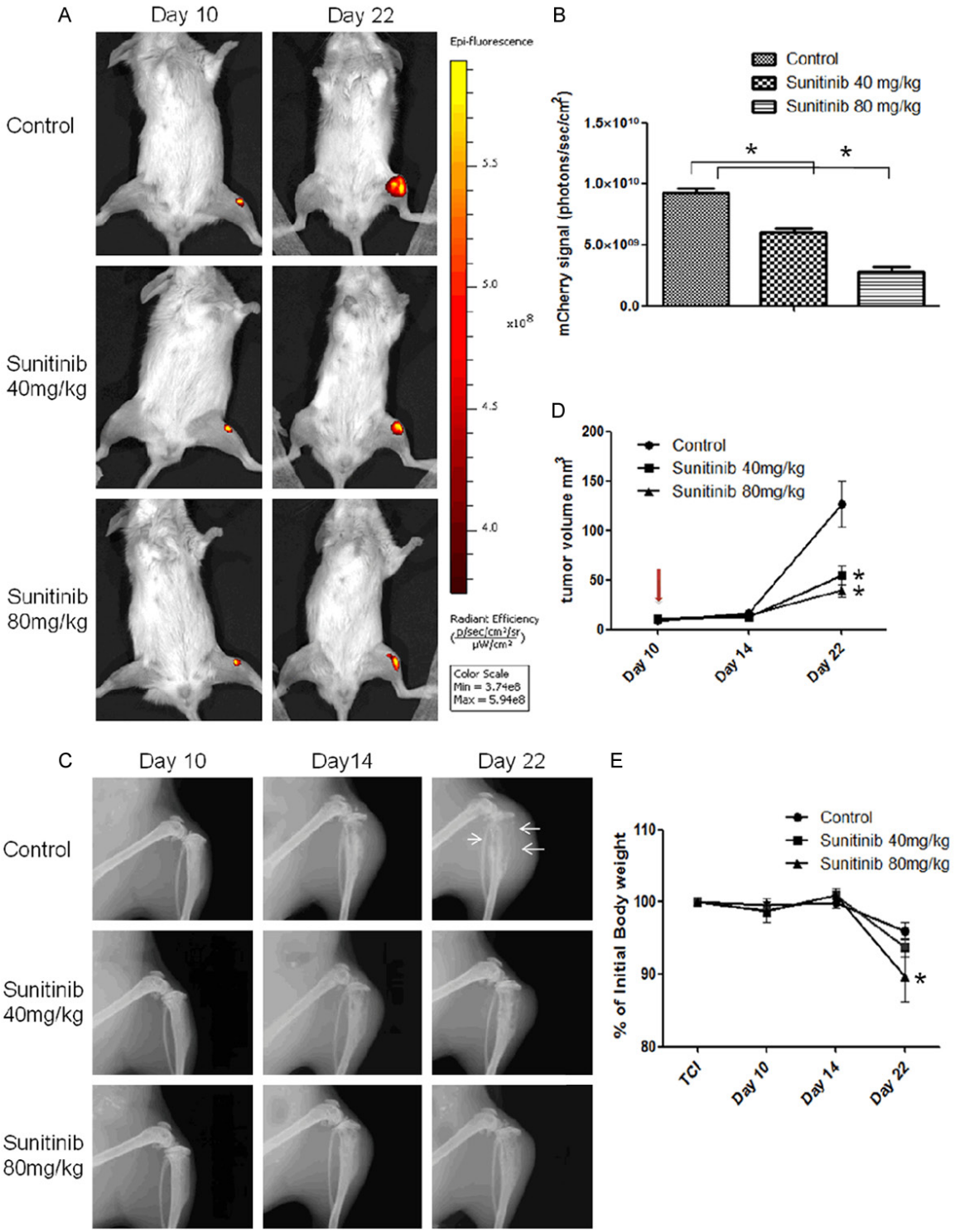

Figure 2. Sunitinib inhibits osteolytic tumor development in a metastasizing intratibial human xenograft OS model in SCID mice. A. Representative images of mCherry fluorescent tumours developing in hind limbs of mice intratibially injected with 143B/LZ+mC cells and treated daily for indicated time periods with CMC solution (control, upper panel), or with 40 mg/kg (middle panel) or 80 mg/kg (lower panel) sunitinib. Colour scale is shown, representing photons/sec. B. Quantitative analysis of mCherry fluorescence of 143B/LZ+mC cell-derived intratibial tumours in mice after 12 days of treatment as indicated. Data are the mean ± SEM of 10 mice analysed per group; $^{*}P<0.05$. C. Representative X-ray images of hind limbs of mice with 143B/LZ+mC cell-derived osteolytic intratibial tumors (arrows) treated for time periods with CMC solution or sunitinib as indicated. D. Effect of sunitinib treatment in primary tumour growth over time in mice intratibially injected with 143B/LZ+mC cells in each of the three group

(n=10) (*P<0.01). E. Body weight of mice treated for indicated time periods with CMC solution or with 40 or 80 mg/kg sunitinib (n=10) (**P<0.001).

ware, Inc., San Diego, CA, USA) was used for the statistical analysis. P<0.05 was considered statistically significant. The data are presented as means ± SEM of the indicated number of independent experiments.

Results

Sunitinib malate inhibits proliferation and provokes apoptosis in OS cell lines in vitro

Effects of the tumour suppressive tyrosine kinase inhibitor sunitinib on proliferation, cell cycle control and apoptosis were studied in osteoblastic SaOS-2 and osteoclastic 143B cells. Treatment of OS cell lines for 24 h with 2 μM and 5 μM sunitinib inhibited proliferation in a dose-dependent manner as assessed by WST-assay (**Figure 1A**) and these results are similar to those observed in *in vitro* studies of other sunitinib-treated tumour cell lines [18]. A flow cytometric cell cycle analysis of SaOS-2 and 143B OS cells treated for 24 h and 48 h with 5 μM revealed a time dependent decrease of percentage of cells in the G1 phase and a concomitant accumulation of cells in the G2 phase (**Figure 1B**). Treatment of SaOS-2 cells with sunitinib increased the percentage of cells in the G2 phase from 16.4% to 30.2% after 24 h and to 56.4% after 48 h of treatment. Similarly, exposure to sunitinib increased the percentage of 143B cells in the G2 phase from 17.3% at 0 h to 21.3% at 24 h and 35.3% after 48 h (Figure S1). To determine whether sunitinib affected the expression levels of the cell cycle proteinscyclin D1 (a protein required for the G1/S transition) and cyclinB1 (a key regulator of the cell transition from G2 to the M phase) qRT-PCR was performed to measure their expression levels in SaOS-2 and 143B cells. In SaOS-2 and 143B cells treated with 5 μM sunitinib there were no significant changes in cyclinD1 expression levels at 48 h as compared to the control, however cyclinB1 levels decreased to 1.5-fold in SaOS-2 cells and 1.2-fold in 143B cells (**Figure 1C**). These results suggested that downregulation of the G2 phase-regulating protein cyclinB1 contributed to sunitinib mediated cell cycle arrest in OS cells leading to apoptosis.

Time dependent enhancement of cell apoptosis by sunitinib was observed in SaOS-2 and 143B cells as indicated by changes in the cell morphology and the cells became round and detached at 72 h (Figure S2). To further confirm that the observed apoptosis was induced by sunitinib, immunoblotting was performed on total cell lysates after sunitinib treatment at 5 μM for 24, 48 and 72 h to detect the activation of caspase-3 and the cleavage of poly (ADP-ribose) polymerase (PARP), which are markers of cells undergoing apoptosis. Sunitinib markedly induced apoptosis in 143B and SaOS-2 cells by increasing the levels of cleaved caspase-3 and cleaved PARP in a time-dependent manner (**Figure 1D**).

Sunitinib malate inhibits the growth of intratibial OS xenografts in mice

The *in vitro* experiments showed that the treatment of OS cell lines with sunitinib inhibited cell growth and provoked apoptosis. Consequently, tumour suppressive effects of sunitinib were studied in SCID mice intratibially injected with 143-B/LZ+mC cells (**Figure 2**). Daily treatment with CMC solution (vehicle control) or with sunitinib was started on day 10 after tumour cell injection when mCherry fluorescence of the intratibial primary tumours became detectable by the IVIS in mice (**Figure 2A**). Sunitinib treatment for 12 days resulted in a significant and dose-dependent reduction of tumour fluorescence in treated compared to control animals (**Figure 2A** and **2B**) consistent with a sunitinib dose-dependent inhibition of intratibial tumor growth over time visualised by x-ray imaging (**Figure 2C**) and assessed by caliper ruler measurements (**Figure 2D**). The mean tumour volume at sacrifice on day 22 assessed by caliper measurements was 126.9±73.1 mm^3 in control animals, and 50.30±36.6 mm^3 or 39.4±20.2 mm^3 in mice treated daily with 40 or 80 mg/kg sunitinib, respectively.

Importantly, the x-ray analysis also showed a notable sunitinib dose-dependent attenuation of osteolysis caused by the developing tumors (**Figure 2C**). Interestingly and presumably as a side effect of the treatment with sunitinib the mice that received 80 mg/kg of the drug per day for 12 days displayed a significant loss of body weight. The loss of body weight was less pronounced and not significant in animals that

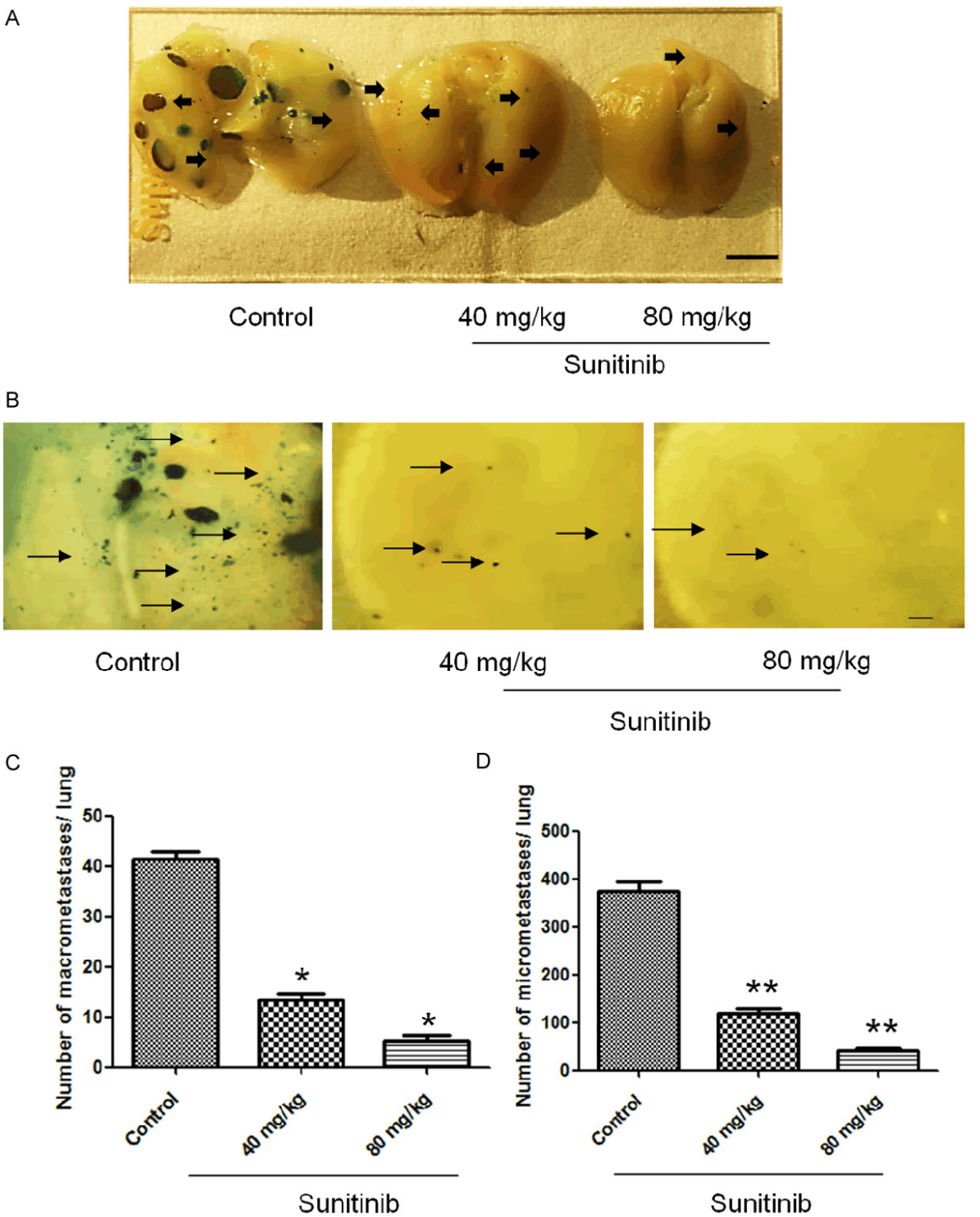

Figure 3. Sunitinib suppresses spontaneous lung metastasis in mice bearing intratibial 143B/LZ+mC cell derived tumours. (A) Representative images of whole mounts of X-gal–stained lungs of mice treated with vehicle (control) or with sunitinib as indicated. The lungs were collected at sacrifice of the mice on day 22 after intratibial inoculation of 143B/LZ+mC cells. The arrowheads point to blue macrometastases (>0.1 mm in largest dimension). Size bar=2 mm. (B) Representative microscopic images of lung micrometastases (<0.1 mm in largest dimension) observed on the whole lung mounts. Arrows point to X-gal–stained lesions. Bars=250 μm. (C) Quantification of macrometastases on the whole mounts of lungs collected from the mice described in (A). (D) Quantification of pulmonary micrometastases. Data in (C and D) are the mean ± SEM numbers of lung macro- and micrometastases per mouse in indicated treatment groups of 10 animals; $^{*}P<0.05$, $^{**}P<0.01$.

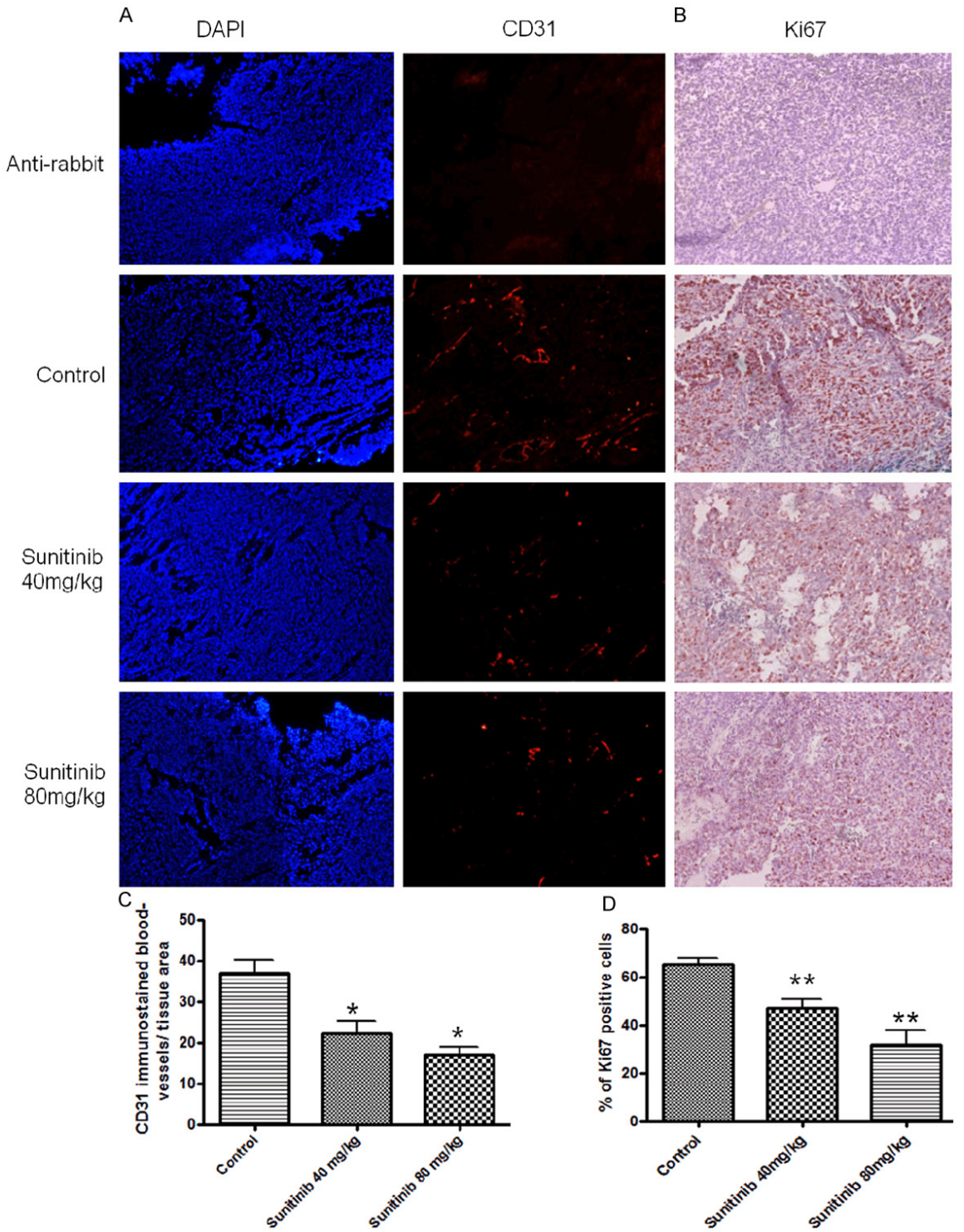

Figure 4. Sunitinib reduces microvessel density and proliferation in intratibial 143B/LZ+mC cell-derived OS xenografts. A. Representative microscopic images (20×) of nuclear DAPI staining (left panels) and of CD31 immunoflourescent staining (right panels) of paraffin sections of primary tumour tissue collected from mice treated with CMC solution alone (control) or with 40 or 80 mg/kg sunitinib. The top right panel shows control immunoflourescent staining with secondary Alexa Fluor 546-labeled antibodies to rabbit IgG (anti-rabbit) alone. B. Representative microscopic images of IHC staining of Ki67 in tumours in paraffin sections of primary tumor tissue of 143B/LZ+mC xenografts treated with control or 40 and 80 mg/kg sunitinib. Scale bars=100 μm. C. Quantitative analysis of microvessel density assessed by CD31 immunoflourescent staining (n=5) $^{*}P<0.005$. D. Quantification of tumour cell proliferation using Ki-67 staining. Data are expressed as Ki-67 positive tumour cells as percentage of total tumour cells. (n=5) $^{**}P<0.002$.

were treated with 40 mg/kg sunitinib per day (**Figure 2E**).

Sunitinib malate suppresses spontaneous pulmonary metastasis of intratibial OS xenografts

To determine whether treatment with sunitinib also influences spontaneous lung metastases formation, metastatic lesions on the lung surface were analysed by X-gal staining after sacrifice of the mice on day 22. Comparison of whole mounts of lungs after x-gal staining revealed an obvious inhibition of macrometastasis in the sunitinib treated groups with respect to the control mice (**Figure 3A**). The mean numbers of macrometastases in the control mice was 40±4.5 per lung while in 40 mg/kg and 80 mg/kg sunitinib-treated mice the mean numbers was 10±4.5 and 3±6.7, respectively (**Figure 3C**). Evaluation of the mean number of X-gal-stained macrometastases on the lung surface revealed a significant decrease by 64% in the 40 mg/kg and 72% in the 80 mg/kg sunitinib treatment groups. Examination at the microscopic level showed that the formation of micrometastases was clearly suppressed in the sunitinib treated groups (**Figure 3B**). The mean number of micrometastases in the control mice was 374±63.8 while in 40 and 80 mg/kg sunitinib the mean numbers was 118.1±35.83 and 35±11.7 per lung, respectively (**Figure 3D**). The micrometastatic lesion was eventually reduced to 66% and 75% in the 40 mg/kg and 80 mg/kg sunitinib treatment group, respectively when compared to the control group.

Sunitinib malate reduces microvessel density and tumour cell proliferation in intratibial OS xenografts

Angiogenesis in intratibial 143-B/LZ+mC cell-derived tumours in vehicle (control) and sunitinib treated mice was examined by CD31 immunoflourescent staining of vascular endothelial cells in paraffin sections of tumour tissue collected at sacrifice. Control tumours were characterised by CD31 positive microvascular endothelium that displayed linked segments of irregular microvessels while the tumours treated with 40 and 80 mg/kg sunitinib a fewer and more isolated CD31 positive microvessels were identified (**Figure 4A**). The mean number of CD31 positive cells in the control mice was 38±7.5 while in 40 mg/kg and 80 mg/kg sunitinib-treated mice the mean numbers were 24±6.5 and 15±4.7, respectively (**Figure 4C**). Quantitative analysis of the density of these microvessel-like structures in dissected tumours revealed a significant decrease of 45% and 54% in mice treated with 40 mg/kg and 80 mg/kg sunitinib, respectively, compared to the control group. In addition, tumour proliferation as determined by Ki67 nuclear antigen staining was analysed in 143-B/LZ+mC cell xenografts from the three groups (**Figure 4B**). The mean number of Ki67 positive cells in the control mice was 63±6.5 while in 40 mg/kg and 80 mg/kg sunitinib-treated mice the mean numbers was 52±7.6 and 38±6.7, respectively (**Figure 4D**). A quantitative analysis of the number of proliferating cells in the tumours collected from mice of the different treatment groups revealed a significant and dose-dependent decrease of Ki67 expressing cells by 52% and 68% in tumours of mice treated with 40 mg/kg and 80 mg/kg sunitinib, respectively, compared to the number of proliferating cells observed in control animals.

Discussion

OS is a rare but devastating disease and metastasizing OS in particular remains largely treatment resistant, reflected by a long-term survival rate of only 20 to 30%. Consequently, novel therapeutics are urgently needed. Previous preclinical studies, which demonstrated that the wide-spectrum kinase inhibitor sunitinib with tumor suppressive activity prevented bone metastasis in renal cell cancer (RCC) and breast cancer mouse models [19, 20], and a recent report on an ongoing clinical trial with sunitinib in a phase II setting (NCT01391962; https://clinicaltrials.gov) in patients suffering from alveolar soft part sarcoma prompted us to investigate in the present study primary tumor and metastasis suppressive effects of sunitinib in a spontaneously metastasizing intratibial human xenograft OS mouse model largely reproducing the human disease.

Initial experiments *in vitro* with the human osteoblastic SaOS-2 and the osteoclastic 143B OS cell lines revealed results similar to those reported from studies with other tumour cell lines treated with sunitinib [18]. Sunitinib significantly and dose-dependently inhibited proliferation and promoted apoptosis. A cell cycle analysis of sunitinib treated cells demonstrated a remarkable increase of a sub-population of

cells in the G2 phase of the cell cycle, suggesting that sunitinib caused a G2/M-arrest, which is in accordance with the findings of other studies investigating sunitinib treated cells [21-23]. The G2/M arrest, which is also consistent with the observed downregulation of cyclinB1 by sunitinib, appears to allow OS cells to enter mitosis andforce them to undergo apoptosis.

The *in vivo* studies in SCID mice were carried out with the osteolytic 143-B/LZ+mC OS cells, which allowed us to access primary tumour growth *in vivo* by monitoring mCherry fluorescence and the detection at the single-cell level of 143-B/LZ+mC cells metastasizing to the lung. Tumour growth over time and osteolysis were comparable to that previously described for 143-B/LZ cells in the intratibial mouse model [24]. Although we were unable to obtain bone density scan data, X-ray imaging showed the expected inhibition of osteolysis in mice with sunitinib.Interestingly, the inhibition of tumour growth in sunitinib treated mice over time observed in the present study was similar to that reported for sunitinib used at comparable doses in xenograft models of triple negative breast cancer and prostate cancer [25-27]. The doses of sunitinib used in this study (40 and 80 mg/kg) were intended to yield serum levels of the drug similar to those reached in a clinical setting in cancer patients [28, 29]. Oral doses of sunitinib at 50-150 mg/kg were also shown to evoke a good tumour response and a manageable toxicity profile in adult patients [28]. Recent studies in patients with metastatic RCC showed that increased doses of sunitinib were well tolerated and further improved the clinical outcome by inhibiting primary tumour growth as well as metastasis [30]. In the present study, mice orally treated with sunitinib showed a significant decrease in the number of primary tumour cells that disseminated to the lung. Since lung metastasis is the main cause of death in OS patients [5], metastasis suppressive efficacy is a major requirement for a novel drug considered to improve the clinical outcome of OS patients. The effect of sunitinib in supressing metastasis has been studied in breast [31, 32] and RCC [22] mouse models.

An important pathophysiological feature of OS is hypervascularisation [33] and VEGF, a key regulator of angiogenesis, is considered as a prognostic marker for poor outcome in OS [34]. This suggests that anti-angiogenic drugs could be beneficial for OS treatment as they may inhibit OS tumour vascularisation. Since anti-angiogenic properties of sunitinib have been reported [11-13] we also looked for effects of sunitinib on blood vessel formation in the primary tumours of our OS mouse model. The observed decrease in MVD in sunitinib treated compared to non-treated control mice suggested that sunitinib targeted regulatory molecules such as VEGFR and inhibited blood vessel formation in this experimental OS model. Importantly and in good agreement with the results of our *in vitro* studies and with the results of studies in xenograft models of colon and prostate cancers [35, 26], sunitinib also reduced significantly the proliferative activity of the intratibial OS primary tumour tissue, which is in line with the observed slower growth of the tumours assessed by mCherry bio-fluorescence imaging and caliper ruler measurements.

A considerable limitation of the relevance of the current study is the fact that the progress of the disease could not be monitored over a longer period of time. Due to the weight loss of mice in response to daily oral sunitinib administration, the animals had to already be sacrificed after 12 days of treatment. Weight loss of mice during administration of sunitinib has been reported in other experimental models [36, 37]. The mechanisms of weight loss due to sunitinib treatment are poorly understood. However, sunitinib has been reported to target fat cells, thereby causing loss of appetite [38]. Thus, the weight loss of sunitinib treated animals observed in the present study might be avoidable in future studies if the animals are put on a high fat diet during sunitinib treatment.

In conclusion, the data of the present study in a spontaneously metastasizing intratibial human xenograft OS mouse model clearly indicate that daily oral administration of sunitinib slowed down tumour growth, reduced primary tumour vascularisation and inhibited the lung metastasis. While the efficacy of sunitinib alone and in combination with other drugs has already been reported in various pre- and clinical studies in other cancer types, our results indicate that sunitinib could also be effective in the treatment for OS.

Acknowledgements

We thank Bernhard Robl, Olga Neklyudova and Knut Husmann for their technical assistance. Our work was supported by the University of Zurich, the Schweizerischer Verein Balgrist (Zurich, Switzerland), the Walter L. & Johanna Wolf Foundation (Zurich, Switzerland), The Highly Specialized Medicine for Musculoskeletal Oncology program of the Canton of Zurich, The Zurcher Krebsliga (Zurich, Switzerland), and The Swiss National Science Foundation SNF Nr.310030_149649.

Disclosure of conflict of interest

None.

Address correspondence to: Ram Mohan Ram Kumar, Department of Orthopaedics, Laboratory for Orthopaedic Research, Balgrist University Hospital, University of Zurich, Zurich, Switzerland. Tel: +41 44 386 3773; Fax: +41 44 386 1669; E-mail: rkumar@research.balgrist.ch

References

[1] Yang J, Zhang W. New molecular insights into osteosarcoma targeted therapy. Curr Opin Oncol 2013; 25: 398-406.

[2] Mirabello L, Troisi RJ, Savage SA. International osteosarcoma incidence patterns in children and adolescents, middle ages and elderly persons. Int J Cancer 2009; 1: 229-34.

[3] Iwamoto Y, Tanaka K, Isu K, Kawai A, Tatezaki S, Ishii T, Kushida K, Beppu Y, Usui M, Tateishi A, Furuse K, Minamizaki T, Kawaguchi N, Yamawaki S. Multiinstitutional phase II study of neoadjuvant chemotherapy for osteosarcoma (NECO study) in Japan: NECO-93J and NECO-95J. J Orthop Sci 2009; 14: 397-404.

[4] Hughes DP. Strategies for the targeted delivery of therapeutics for osteosarcoma. Expert Opin Drug Deliv 2009; 6: 1311-21.

[5] Rasalkar DD, Chu WC, Lee V, Paunipagar BK, Cheng FW, Li CK. Pulmonary metastases in children with osteosarcoma: characteristics and impact on patient survival. Pediatr Radiol 2011; 2: 227-36.

[6] Blay JY. Chemotherapy for osteosarcoma without high-dose methotrexate: another piece in the puzzle. Onkologie 2007; 30: 226-7.

[7] Chou AJ, Gorlick R. Chemotherapy resistance in osteosarcoma: current challenges and future directions. Expert Rev Anticancer Ther 2006; 6: 1075-85.

[8] Chow LQ, Eckhardt SG. Sunitinib: From Rational Design to Clinical Efficacy. J Clin Oncol 2007; 7: 884-96.

[9] Mendel DB, Laird AD, Xin X, Louie SG, Christensen JG, Li G, Schreck RE, Abrams TJ, Ngai TJ, Lee LB, Murray LJ, Carver J. In vivo antitumour activity of SU11248, a novel tyrosine kinase inhibitor targeting vascular endothelial growth factor and platelet-derived growth factor receptors: determination of a pharmacokinetic/pharmacodynamic relationship. Clin Cancer Res 2003; 9: 327-37.

[10] Andrae N, Kirches E, Hartig R, Haase D, Keilhoff G, Kalinski T, Mawrin C. Sunitinib targets PDGF-receptor and Flt3 and reduces survival and migration of human meningioma cells. Eur J Cancer 2012; 12: 1831-41.

[11] Raymond E, Hammel P, Dreyer C, Maatescu C, Hentic O, Ruszniewski P, Faivre S. Sunitinib in pancreatic neuroendocrine tumours. Target Oncol 2012; 2: 117-25.

[12] Motzer RJ, Hutson TE, Tomczak P. Sunitinib versus interferon alpha in metastatic renal-cell carcinoma. N Engl J Med 2006; 356: 115-24.

[13] Younus J, Verma S, Franek J, Coakley N. Sunitinib malate for gastrointestinal stromal tumour in imatinibmesylate-resistant patients: recommendations and evidence. Curr Oncol 2010; 4: 4-10.

[14] Steinmann P, Walters DK, Arlt MJ, Banke IJ, Ziegler U, Langsam B, Arbiser J, Muff R, Born W, Fuchs B. Antimetastatic activity of honokiol in osteosarcoma. Cancer 2012; 118: 2117-2127.

[15] Zhang C, Yang L, Wang XB, Wang JS, Geng YD, Yang CS, Kong LY. Calyxin Y induces hydrogen peroxide-dependent autophagy and apoptosis via JNK activation in human non-small cell lung cancer NCI-H460 cells. Cancer Lett 2013; 340: 51-62.

[16] Arlt MJ, Banke IJ, Walters DK, Puskas GJ, Steinmann P, Muff R, Born W, Fuchs B. LacZ transgene expression in the subcutaneous Dunn/LM8 osteosarcoma mouse model allows for the identification of micrometastasis. J Orthop Res 2011; 6: 938-46.

[17] Reidy K, Campanile C, Muff R, Born W, Fuchs B. mTHPC-mediated photodynamic therapy is effective in the metastatic human 143B osteosarcoma cells. Photochem Photobiol 2012; 3: 721-7.

[18] de Boüard S, Herlin P, Christensen J, Lemoisson E, Gauduchon P, Raymond E, Guillamo J. Antiangiogenic and anti-invasive effects of sunitinib on experimental human glioblastoma. Neuro Oncol 2007; 9: 412-42310.

[19] Maita S, Yuasa T, Tsuchiya N, Mitobe Y, Narita S, Horikawa Y, Hatake K, Fukui I, Kimura S, Maekawa T, Habuchi T. Antitumor effect of sunitinib against skeletal metastatic renal cell carcinoma through inhibition of osteoclast function. Int J Cancer 2012; 3: 677-84.

[20] Murray LJ, Abrams TJ, Long KR. SU11248 inhibits tumor growth and CSF-1R-dependent osteolysis in an experimental breast cancer

bone metastasis model. Clin Exp Metastasis 2003; 20: 757-766.
[21] Martinho O, Silva-Oliveira R, Miranda-Gonçalves V, Clara C, Almeida JR, Carvalho AL, Barata JT, Reis RM. In Vitro and In Vivo Analysis of RTK Inhibitor Efficacy and Identification of Its Novel Targets in Glioblastomas. Transl Oncol 2013; 2: 187-96.
[22] Wu CL, Ping SY, Yu CP, Yu DS. Tyrosine kinase receptor inhibitor-targeted combined chemotherapy for metastatic bladder cancer. Kaohsiung J Med Sci 2012; 4: 194-203.
[23] Andrae N, Kirches E, Hartig R, Haase D, Keilhoff G, Kalinski T, Mawrin C. Sunitinib targets PDGF-receptor and Flt3 and reduces survival and migration of human meningioma cells. Eur J Cancer 2012; 12: 1831-41.
[24] Brennecke P, Arlt MJ, Campanile C, Husmann K, Gvozdenovic A, Apuzzo T, Thelen M, Born W, Fuchs B. CXCR4 antibody treatment suppresses metastatic spread to the lung of intratibial human osteosarcoma xenografts in mice. Clin Exp Metastasis 2014; 3: 339-49.
[25] Chinchar E, Makey KL, Gibson J, Chen F, Cole SA, Megason GC, Vijayakumar S, Miele L, Gu JW. Sunitinib significantly suppresses the proliferation, migration, apoptosis resistance, tumour angiogenesis and growth of triple-negative breast cancers but increases breast cancer stem cells. Vasc Cell 2014; 6: 12.
[26] Cumashi A, Tinari N, Rossi C, Lattanzio R, Natoli C, Piantelli M, Iacobelli S. Sunitinib malate (SU-11248) alone or in combination with low-dose docetaxel inhibits the growth of DU-145 prostate cancer xenografts. Cancer Lett 2008; 2: 229-33.
[27] Denorme M, Yon L, Roux C, Gonzalez BJ, Baudin E, Anouar Y, Dubessy C. Both sunitinib and sorafenib are effective treatments for pheochromocytoma in a xenograft model. Cancer Lett 2014; 2: 236-44
[28] Faivre S, Delbaldo C, Vera K, Robert C, Lozahic S, Lassau N, Bello C, Deprimo S, Brega N, Massimini G, Armand JP, Scigalla P, Raymond E. Safety, pharmacokinetic, and antitumor activity of SU11248, a novel oral multitarget tyrosine kinase inhibitor, in patients with cancer. J Clin Oncol 2006; 1: 25-35.
[29] Mendel DB, Laird AD, Xin X, Louie SG, Christensen JG, Li G, Schreck RE, Abrams TJ, Ngai TJ, Lee LB, Murray LJ, Carver J, Chan E, Moss KG, Haznedar JO, Sukbuntherng J, Blake RA, Sun L, Tang C, Miller T, Shirazian S, McMahon G, Cherrington JM. In vivo antitumor activity of SU11248, a novel tyrosine kinase inhibitor targeting vascular endothelial growth factor and platelet-derived growth factor receptors: determination of a pharmacokinetic/pharm-acodynamic relationship. Clin Cancer Res 2003; 1: 327-37.
[30] Buti S, Donini M, Lazzarelli S, Passalacqua R. A new modified schedule of sunitinib for metastatic renal cell carcinoma: a retrospective analysis. Acta Biomed 2012; 83: 88-94.
[31] Kodera Y, Katanasaka Y, Kitamura Y, Tsuda H, Nishio K, Tamura T, Koizumi F. Sunitinib inhibits lymphatic endothelial cell functions and lymph node metastasis in a breast cancer model through inhibition of vascular endothelial growth factor receptor 3. Breast Cancer Res 2011; 13: R66.
[32] Tanaka Y, Shibata MA, Morimoto J, Otsuki Y. Sunitinib suppresses tumour growth and metastases in a highly metastatic mouse mammary cancer model. Anticancer Res 2011; 4: 1225-34.
[33] Kubo T, Shimose S, Fujimori J, Arihiro K, Ochi M. Diversity of angiogenesis among malignant bone tumours. Mol Clin Oncol 2013; 1: 131-136.
[34] Bajpai J, Sharma M, Sreenivas V, Kumar R, Gamnagatti S, Khan SA, Rastogi S, Malhotra A, Bakhshi S. VEGF expression as a prognostic marker in osteosarcoma. Pediatr Blood Cancer 2009; 6: 1035-9.
[35] Gotink KJ, Broxterman HJ, Honeywell RJ, Dekker H, de Haas RR, Miles KM, Adelaiye R, Griffioen AW, Peters GJ, Pili R, Verheul HM. Acquired tumor cell resistance to sunitinib causes resistance in a HT-29 human colon cancer xenograft mouse model without affecting sunitinib biodistribution or the tumor microvasculature. Oncoscience 2014; 1: 844-853.
[36] Zhou Q, Gallo JM. Differential effect of sunitinib on the distribution of temozolomide in an orthotopic glioma model. Neuro Oncol 2009; 3: 301-10.
[37] Tanaka Y, Shibata MA, Morimoto J, Otsuki Y. Sunitinib suppresses tumour growth and metastases in a highly metastatic mouse mammary cancer model. Anticancer Res 2011; 4: 1225-34.
[38] Jian-Wei Gu, Kristina L Makey, Edmund Chinchar, Carissa Howie and Lucio Miele. Angiogenesis inhibitor, Sunitinib significantly reduces adipose tissue mass in high fat diet-induced postmenopausal obese mice. FASEB J 2013; 27: 1154-9.

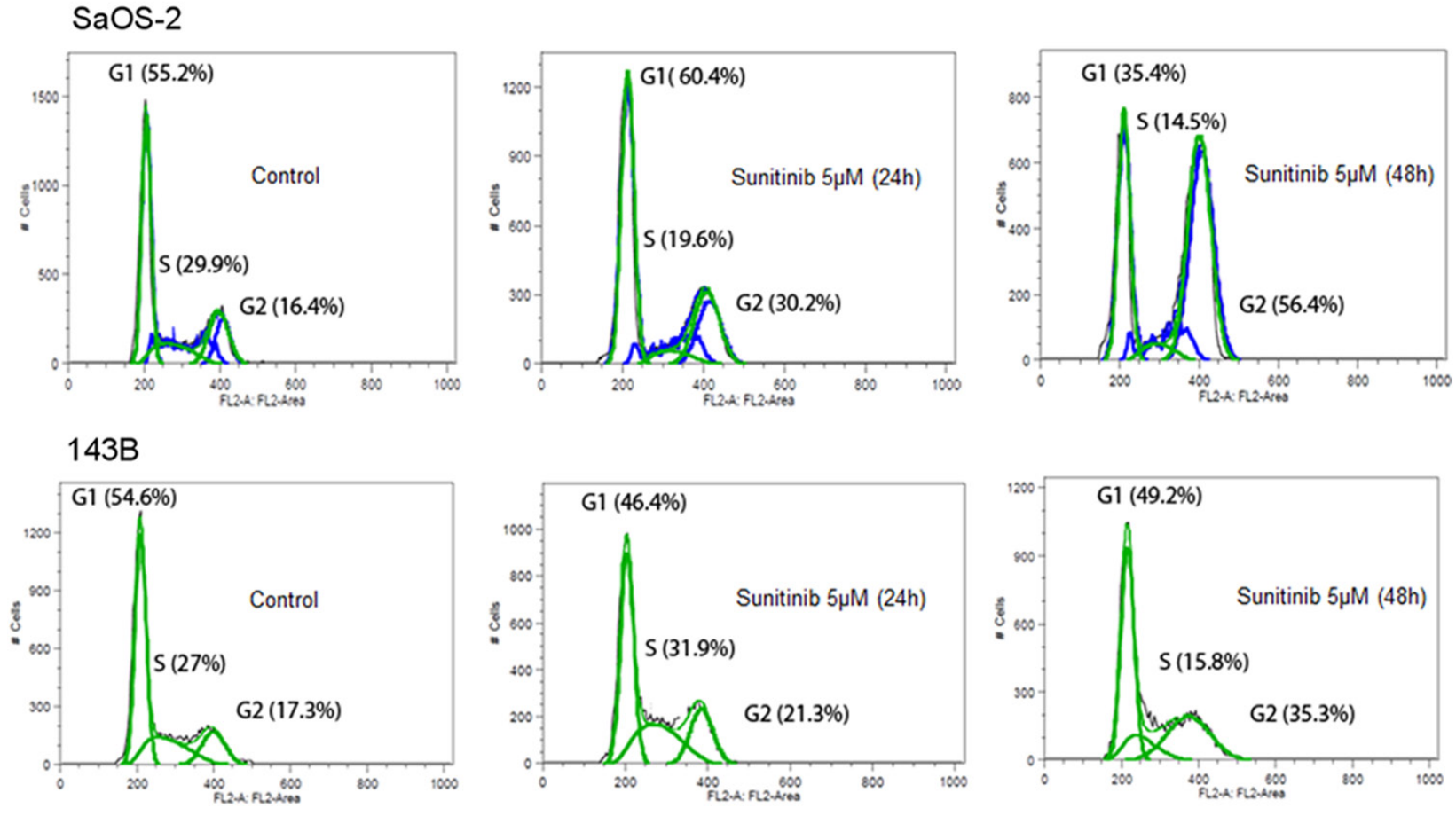

Figure S1. Cell cycle analysis of SaOS-2 and 143B cells treated with sunitinib. Cell cycle analysis of SaOS-2 and 143B cells treated with sunitinib. Effects of the treatment of SaOS-2 and 143B cells for 24 h with 5 μM sunitinib on the cell cycle were evaluated by propidium iodide (PI) staining of the cells and subsequent FACS analysis.

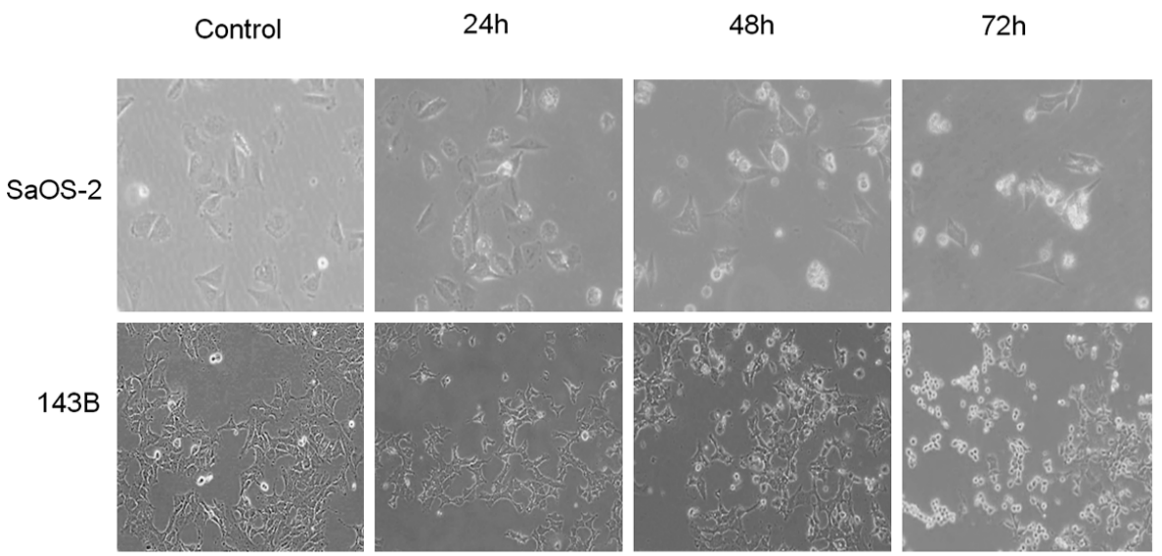

Figure S2. Phase contrast microscopic images of SaOS-2 and 143B cells treated with sunitinib for indicated time periods.